ARMY RESEARCH LABORATORY

Evaluation of an Al, La Modified $MgZn_2Y_2$ Alloy

by Vincent H. Hammond, Tomoko Sano, Joseph P. Labukas, Teresa A. Dillon, Brady G. Butler, Jianghua Shen, and Qiuming Wei

ARL-TR-6807 **February 2014**

NOTICES

Disclaimers

The findings in this report are not to be construed as an official Department of the Army position unless so designated by other authorized documents.

Citation of manufacturer's or trade names does not constitute an official endorsement or approval of the use thereof.

Destroy this report when it is no longer needed. Do not return it to the originator.

Army Research Laboratory
Aberdeen Proving Ground, MD 21005-5069

ARL-TR-6807 **February 2014**

Evaluation of an Al, La Modified $MgZn_2Y_2$ Alloy

Vincent H. Hammond, Tomoko Sano, Joseph P. Labukas, Teresa A. Dillon, and Brady G. Butler
Weapons and Materials Research Directorate, ARL

Jianghua Shen and Qiuming Wei
University of North Carolina - Charlotte

REPORT DOCUMENTATION PAGE	Form Approved OMB No. 0704-0188

1. REPORT DATE *(DD-MM-YYYY)*	2. REPORT TYPE	3. DATES COVERED (From - To)
February 2014	Final	1 August 2012–31 December 2013

4. TITLE AND SUBTITLE
Evaluation of an Al, La Modified $MgZn_2Y_2$ Alloy

5a. CONTRACT NUMBER

5b. GRANT NUMBER

5c. PROGRAM ELEMENT NUMBER

6. AUTHOR(S)
Vincent H. Hammond, Tomoko Sano, Joseph P. Labukas, Teresa A. Dillon, Brady G. Butler, Jianghua Shen,* and Qiuming Wei*

5d. PROJECT NUMBER

5e. TASK NUMBER

5f. WORK UNIT NUMBER

7. PERFORMING ORGANIZATION NAME(S) AND ADDRESS(ES)
U.S. Army Research Laboratory
ATTN: RDRL-WMM-F
Aberdeen Proving Ground, MD 21005-5069

8. PERFORMING ORGANIZATION REPORT NUMBER
ARL-TR-6807

9. SPONSORING/MONITORING AGENCY NAME(S) AND ADDRESS(ES)

10. SPONSOR/MONITOR'S ACRONYM(S)

11. SPONSOR/MONITOR'S REPORT NUMBER(S)

12. DISTRIBUTION/AVAILABILITY STATEMENT
Approved for public release; distribution is unlimited.

13. SUPPLEMENTARY NOTES
*Department of Mechanical Engineering and Engineering Science, University of North Carolina-Charlotte, Charlotte, NC.

14. ABSTRACT
Magnesium alloys are of interest due to their potential for significant light-weighting in both vehicle and personnel related applications. In this report, a relatively new alloy obtained from Japan was evaluated for its mechanical and electromechanical properties. Although the alloy displayed promising mechanical properties, the corrosion resistance of the alloy was found to fall well below that of other magnesium alloys recently evaluated at the U.S. Army Research Laboratory/Weapons and Materials Research Directorate (ARL/WMRD).

15. SUBJECT TERMS
magnesium, mechanical properties, corrosion

16. SECURITY CLASSIFICATION OF:			17. LIMITATION OF ABSTRACT	18. NUMBER OF PAGES	19a. NAME OF RESPONSIBLE PERSON
a. REPORT	b. ABSTRACT	c. THIS PAGE			Vincent H. Hammond
Unclassified	Unclassified	Unclassified	UU	28	19b. TELEPHONE NUMBER (*Include area code*) (410) 306-4961

Standard Form 298 (Rev. 8/98)
Prescribed by ANSI Std. Z39.18

Contents

List of Figures

List of Tables

Acknowledgments

The authors would like to express their appreciation to Dr. Jian Yu, Micah Gallagher, and James Catalano for their support in sample preparation and testing.

1. Background and Technical Objectives

In 2001, Inoue et al. announced the development of a $MgZn_1Y_2$ alloy with a yield strength over 600 MPa while maintaining a ductility of 5% (*1*). The high strength of the alloy, which was prepared by extruding spray atomized powders at 300 °C, was attributed to a fine grain size, the fine dispersion of $Mg_{24}Y_5$ particles, and the presence of a long period stacking ordered (LPSO) structure consisting of a solid solution of yttrium (Y) and zinc (Zn) atoms arranged in alternating layers of Mg and an intermetallic phase. For the $MgZn_1Y_2$ alloys, the LPSO phase has been nominally identified as $Mg_{12}ZnY$ (*2*). A subsequent study has indicated that dramatic strength of the alloy may be attributed, in part, to the LPSO phase strongly accelerating the refinement of Mg grains during extrusion (*3*). It was also demonstrated in this study that the well aligned LPSO phase in the extruded alloy acts as a short-fiber reinforcement that further strengthens the alloy (*3*). Finally, a study on the $MgZn_1RE_2$ alloy (in which RE = rare-earth element) determined that the best RE for improving overall mechanical properties were Y, gadolinium (Gd), and terbium (Tb) (*4*). However, of these, only Y is a realistic alloying addition due to economic considerations.

As could be expected, the announcement of this alloy resulted in numerous research efforts that used variations on the Zn:Y ratio in an effort to identify alloys with even higher strengths. Although the strengths of these new alloys were not as high as those reported by Inoue, the properties were still noteworthy. For example, a $MgZn_2Y_2$ sheet was found to have a yield strength of 319 MPa, an ultimate tensile strength of 340 MPa, and an 11% elongation (*5*). Further increasing the Y and Zn content by an additional percent (e.g., $MgZn_3Y_3$) resulted in an ultimate tensile strength over 400 MPa with an elongation of 8% (5). In an effort to develop alloys with acceptable corrosion resistance, additional studies have demonstrated that the addition of Al or La to the $MgZn_2Y_2$ alloy results in the formation of a thin, dense, and uniform surface layer that improves the corrosion performance of the alloy (*6-8*).

Due to their light weight and high-specific properties, Mg alloys are of interest to the U.S. Army for a broad variety of structural and protection related applications in vehicle platforms as well as personnel equipment. Although a majority of ongoing efforts at the U.S. Army Research Laboratory (ARL) focus on improving mechanical and electrochemical (corrosion) performance, new Mg alloys are routinely evaluated in order to determine their potential for use in the Army systems and/or platforms. As a result, the purpose of this study was to evaluate the mechanical and electrochemical performance of a $MgZn_2Y_2$ alloy with minor Al and La additions to other Mg alloys recently evaluated by ARL.

2. Material Characterization

Two extruded alloy rods were received from Fuji Light Metal Company (Nagasu, Japan) through the efforts of the U.S. Army International Technology Center Pacific office. For ease of discussion and to ease identification, the alloy will be referred to as the Fuji Light alloy. The samples were from the same extrusion and had a diameter of 22 mm and an overall length of 500 mm. No additional details regarding the processing of the rods were provided. The composition and tensile properties of the alloy as provided by the manufacturer are listed in table 1.

Table 1. Alloy composition and strength properties provided by Fuji Light Metals Company.

	Mg	**Zn**	**Y**	**Al**	**La**
Atomic %	Bal	1.98	1.99	0.36	0.10
Weight %	Bal	4.88	6.67	0.37	0.52
Yield Stress 353 MPa		Tensile Strength 420 MPa		Elongation 5%	

Metallographic samples were taken from the end of the rod as well as from the transverse (normal to extrusion) direction. The samples were subjected to coarse and fine grinding followed by subsequently finer polishing steps starting at 3-µm diamond suspension and finishing with 0.05-µm colloidal silica. This procedure has proven successful in achieving a high-quality surface in a variety of Mg alloys (*9*).

Microstructural characterization was conducted with a Hitachi S4700 scanning electron microscope (SEM) and the FEI Nova NanoSEM 600 microscope. SEM micrographs of samples taken from the end of the rod as well as the transverse direction are shown in figure 1. The micrographs reveal a complex microstructure with a high volume of precipitates. As expected, micrographs taken in the transverse direction reveal an elongated precipitate structure due to the extrusion of the samples. The fibrous (or semicontinuous) precipitates are the LPSO phase that has been reported in these alloy systems (*5*, *10*, *11*).

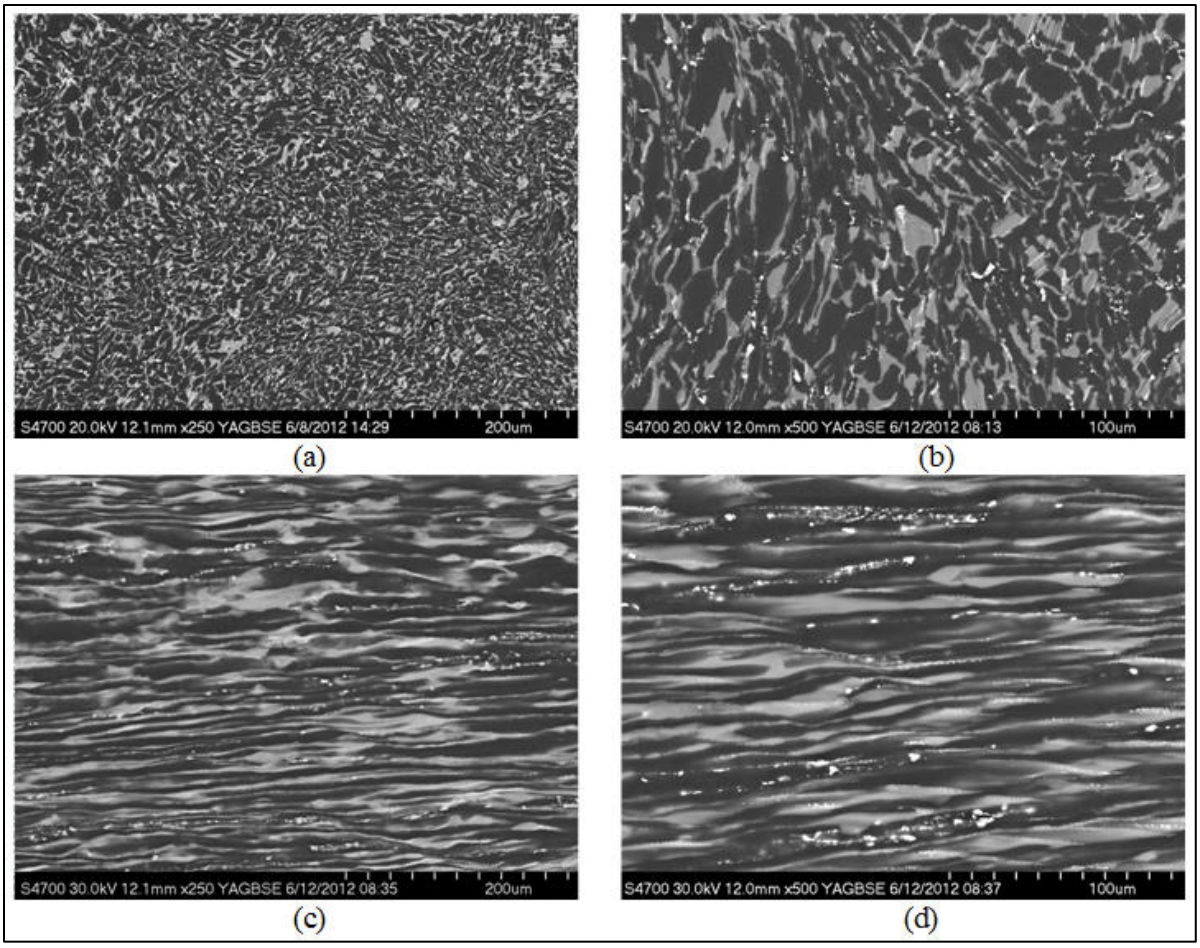

Figure 1. Scanning electron micrographs of the as-extruded microstructure in the Fuji Light alloy. Images in (a, b) are along the longitudinal direction, while those in (c, d) are taken in transverse direction.

Energy dispersive spectroscopy (EDS) was used to determine the approximate elemental content of various phases in the microstructure. Results provided in figure 2 indicate that the matrix (region 1) is primarily Mg with a small amount of Y and Zn. Region 2 in the micrograph is a region of the LPSO precipitate found in these alloys. The Y and Zn content in the precipitates appears to be several times higher than that of the matrix. The La is uniformly distributed in the matrix and two precipitates. In contrast, the Al appears to be found primarily in the bright white precipitates. More detailed analysis is needed to fully determine the elemental distribution that occurs in these alloys.

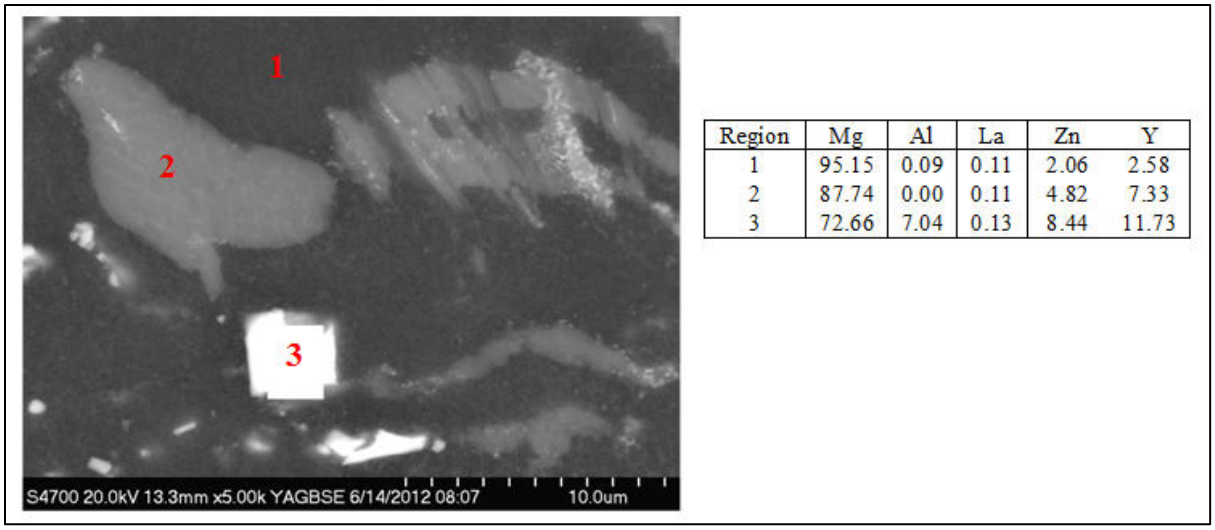

Region	Mg	Al	La	Zn	Y
1	95.15	0.09	0.11	2.06	2.58
2	87.74	0.00	0.11	4.82	7.33
3	72.66	7.04	0.13	8.44	11.73

Figure 2. EDS of sample taken from the longitudinal direction. Region 1 is the matrix, region 2 is the LPSO phase, and region 3 is an Al containing precipitate. Amounts are given in atomic percent.

Phase and texture analysis of the as-extruded sample was measured on a PW3050/60 X'Pert PRO PANalytical MPD x-ray diffractometer using CuKα ($\lambda = 0.1542$ nm) radiation. The scan was conducted from 20° to 120° with a 0.052° step and 186 s dwell. Peak analysis of the x-ray diffraction profile (figure 3) indicated the presence of α-Mg, $Mg_3Zn_3Y_2$, Al_2Y_3, and $Al_2Y_3(AlO_4)_3$ (compounds listed in extent of appearance). This is in general agreement with an earlier report that found that $MgZn_2Y_2$ alloys were composed of an α-Mg phase, an $Mg_{12}ZnY$ LPSO phase, and the $Mg_3Zn_3Y_2$ compound (*2*). Following the pattern (figure 3) is table 2 that details the compound(s) associated with a given peak. As expected, the majority of peaks are associated with pure Mg. A representative pole figure (shown in figure 4) for the basal (002) plane clearly indicates a highly textured structure with the poles for the basal planes aligned normal to the extrusion direction (e.g., the basal planes are parallel to the extrusion direction).

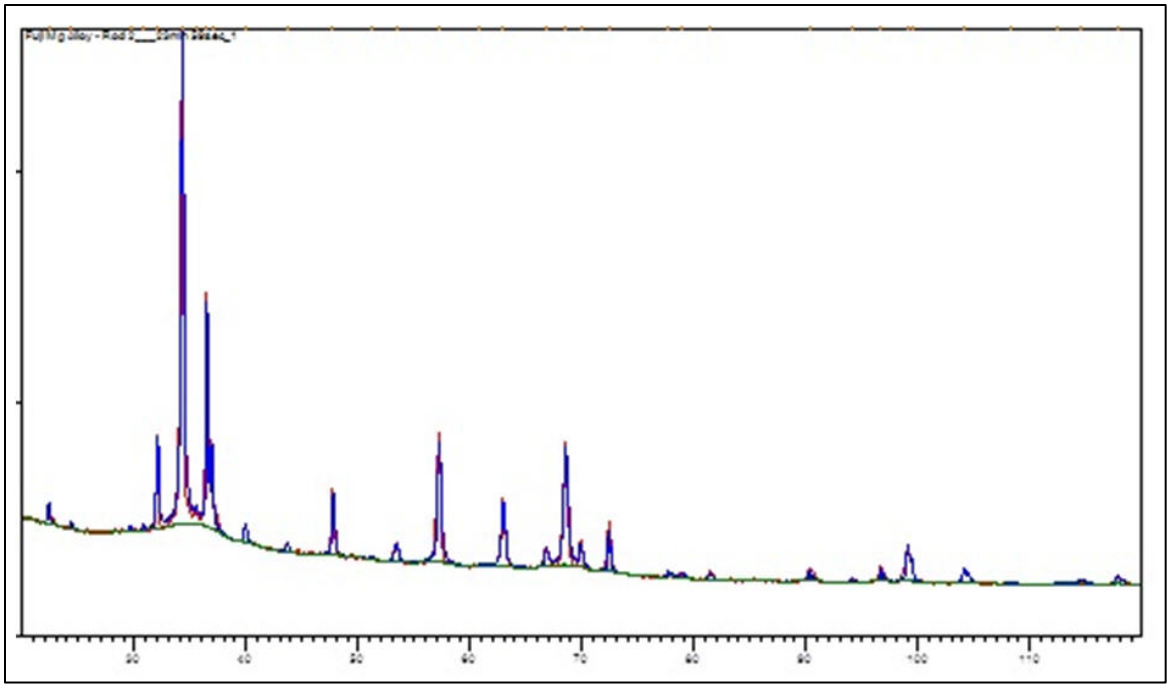

Figure 3. X-ray diffraction pattern for the alloy.

Table 2. Compounds corresponding to major peaks observed in x-ray diffraction pattern.

2 Theta	**Matched By**	**2 Theta**	**Matched By**
22.3089	$Mg_3Zn_3Y_2$	68.4777	Mg; Al_2Y_3
24.3777	Al_2Y_3	69.8657	Mg; $Al_2Y_3(AlO_4)_3$
32.0590	Mg; Al_2Y_3	72.3498	Mg; Al_2Y_3; $Al_2Y_3(AlO_4)_3$
34.2687	Mg	77.7120	Mg; Al_2Y_3; $Al_2Y_3(AlO_4)_3$
36.4995	Mg; Al_2Y_3	78.8797	$Mg_3Zn_3Y_2$; Al_2Y_3; $Al_2Y_3(AlO_4)_3$
36.9542	$Mg_3Zn_3Y_2$; Al_2Y_3; $Al_2Y_3(AlO_4)_3$	81.4174	Mg; $Al_2Y_3(AlO_4)_3$
39.8987	$Al_2Y_3(AlO_4)_3$	90.3253	Mg; $Mg_3Zn_3Y_2$; Al_2Y_3
43.6628	$Mg_3Zn_3Y_2$	94.1478	Mg; Al_2Y_3
47.7131	Mg; Al_2Y_3; $Al_2Y_3(AlO_4)_3$	96.6882	Mg; Al_2Y_3
53.3643	$Mg_3Y_2Zn_3$; $Al_2Y_3(AlO_4)_3$	99.0664	Mg; Al_2Y_3
57.2301	Mg; Al_2Y_3	104.1390	Mg; Al_2Y_3
62.9434	Mg; $Al_2Y_3(AlO_4)_3$	117.8176	Mg
66.7551	$Mg_3Zn_3Y_2$; Al_2Y_3; $Al_2Y_3(AlO_4)_3$	—	—

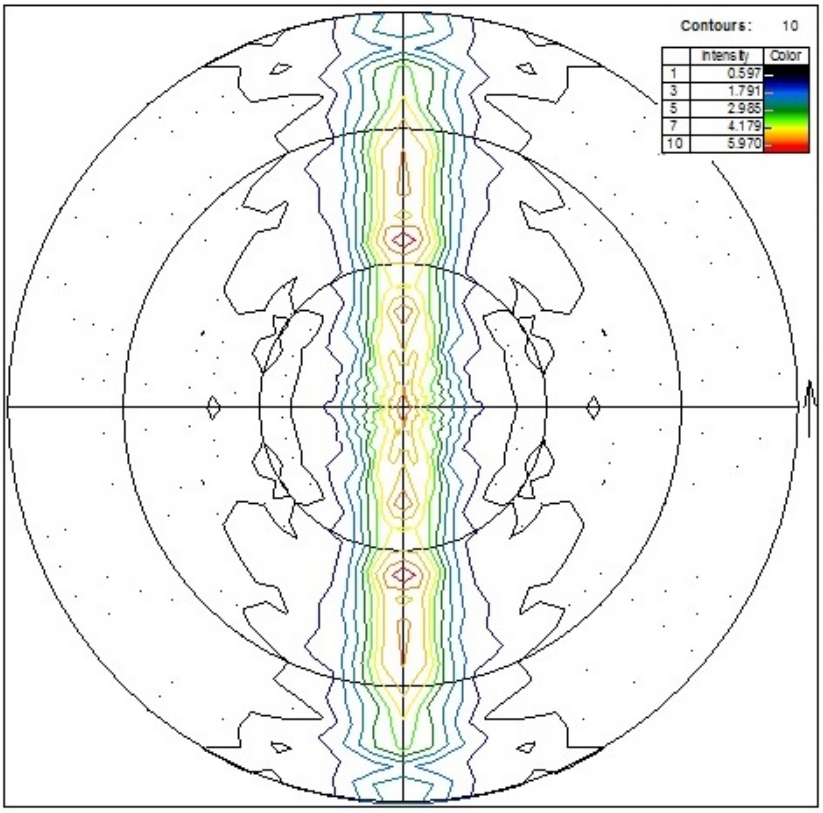

Figure 4. The (002) pole figure for extruded rod. Extrusion direction is left to right.

3. Mechanical Testing

Tensile testing was performed on samples taken from the longitudinal direction of the extruded rods. Total sample length was 40 mm, with a gage section of 12 mm long, 2 mm wide, and 0.8 mm thick. The displacement rate was 0.1 mm/min for sample 1, 0.5 mm/min for sample 2, and 0.3 mm/min for samples 3, 4, and 5. Rate dependence was not observed for these samples. Test results shown in figure 5 indicate a yield strength of approximately 350 MPa and an ultimate strength of approximately 400 MPa. There was a broad distribution in the total elongation of the samples, ranging from a low of approximately 5% to a high of 15%. In general, these values are in good agreement with those provided by the supplier (see table 1).

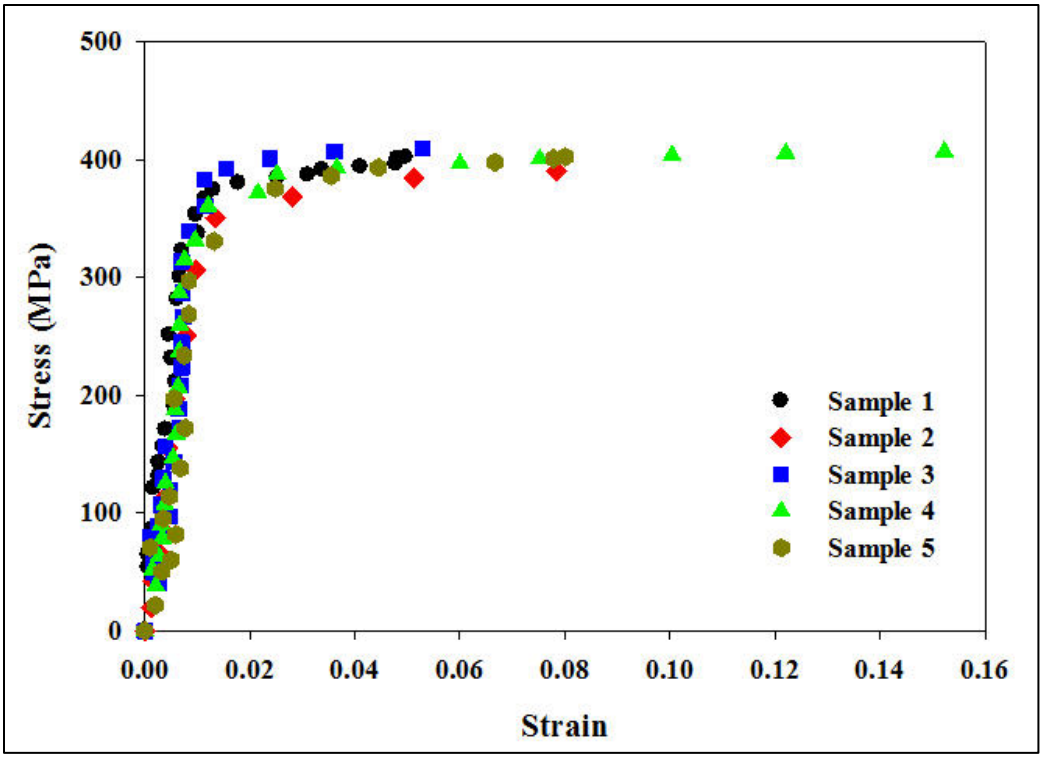

Figure 5. Tensile stress strain curves obtained from multiple samples of the Fuji Light alloy. A consistent behavior is observed across multiple strain rates.

Failure surfaces at various magnifications and directions are shown in figure 6. In general, the micrographs reveal a dimpled fracture surface indicative of ductile behavior, although there appears to be a small region of brittle cleavage failure (figure 6a). A closer examination of the fracture surface (6b) indicates that particle fracture also occurred. This observation is confirmed by the micrograph in 6e in which a fractured particle on the sample surface can be seen. Micrographs in figures 6c and d were taken of the sample surface near the fracture plane and illustrate how the LPSO phase (light gray phase) can act as short fiber reinforcements (*3*). Indeed, a study on a $MgZn_1Y_2$ alloy demonstrated that the LPSO phase was the primary cause of an observed orientation dependence in the yield stress (*3*).

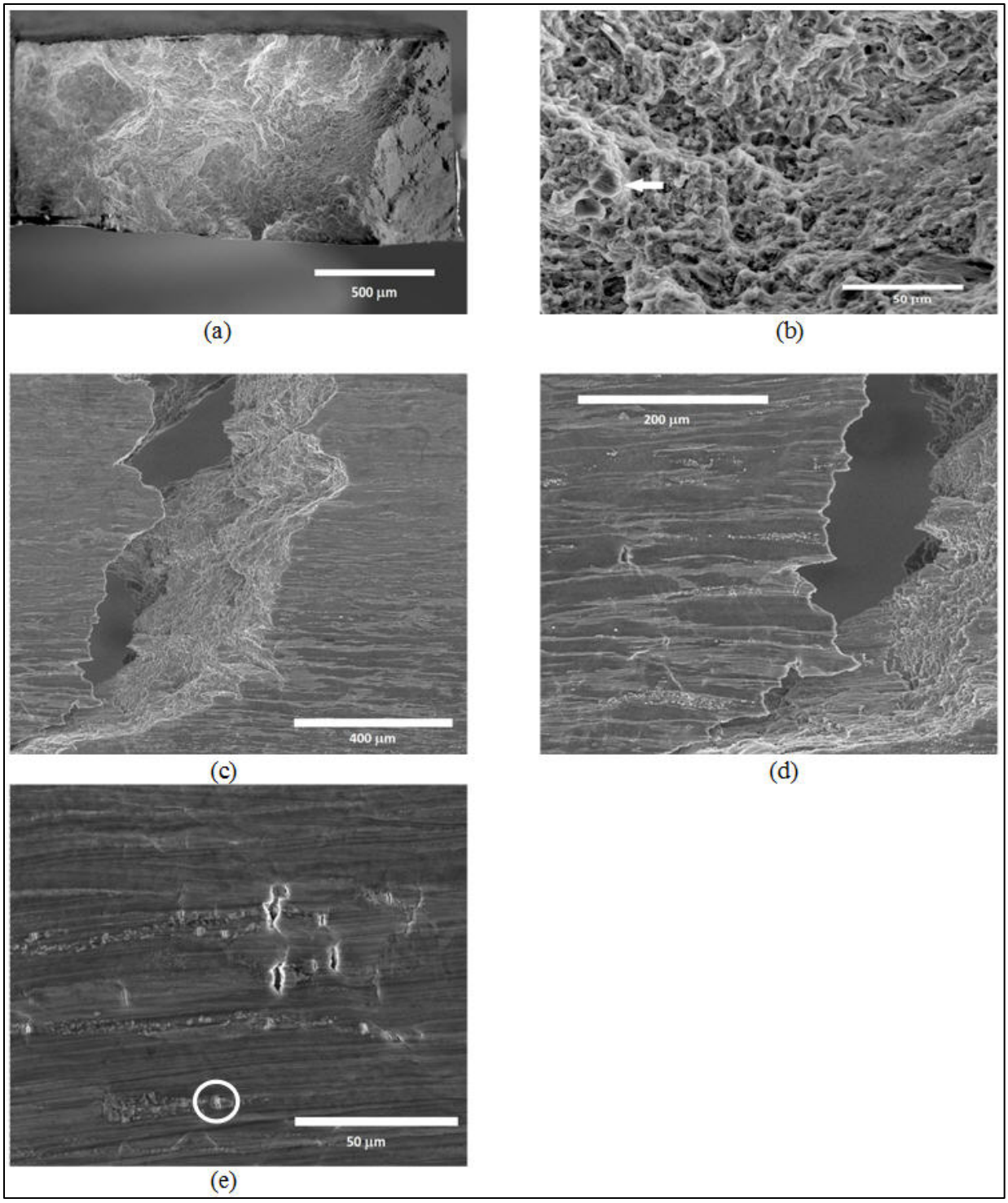

Figure 6. Micrographs of tensile fracture surfaces: (a) entire fracture surface, showing generally ductile failure, with cleavage failure on one side; (b) higher magnification image showing failed precipitates; (c, d) images of the sample surfaces showing how LPSO phase can act as short fiber reinforcements; and (e) image of sample surface showing fractured precipitate.

Room temperature compression tests were performed at both quasi-static (strain rate approximately 10^{-3} s^{-1}) and dynamic (strain rate approximately 10^{3} s^{-1}) conditions. Samples were cut from the two extruded rods along the longitudinal (flow) and transverse directions and labeled accordingly. Sample dimensions were 2.5 mm × 2.5 mm × 5.0 mm (quasi-static) and 2.5 mm × 2.5 mm × 2.0 mm (dynamic). Quasi-static tests were performed on a MTS 810 hydro-servo system while the dynamic tests were conducted on a split Hopkinson pressure bar (Kolsky bar) system. For all tests, grease was applied to both loading faces of the samples to mitigate friction. The prescribed quasi-static strain rates were achieved by controlling the speed of the cross-head whereas control of the dynamic strain rates was realized by the gas pressure. Three independent tests were conducted for each condition.

Typically, single phase Mg alloys, such as AZ31B, display a large degree of anisotropy when tested in tension and compression. In the majority of cases, the alloy has a much lower yield stress in compression compared to tensile loading. However, the ultimate strength is oftentimes much higher in compression. This directional dependence is primarily the result of twinning that occurs during loading due to the limited slip systems available at room temperature in the hexagonal close-packed crystal structure. In the case of extruded samples, twinning can occur when a compressive load is applied parallel to the extrusion direction (*12*, *13*).

Comparison of the quasi-static results (figures 5, 7) indicates similar yield strengths in tension and compression (approximately 400 MPa) for samples tested parallel to the extrusion direction. In contrast, the yield strength of AZ31B is approximately 100 MPa in compression. The effective increase in the compressive yield strength (relative to a non-LPSO containing alloy) has been attributed to the grain refinement that occurs during extrusion due to the presence of the LPSO phase (*14*). The refined grain structure served to hinder the formation of twins in the matrix. In addition, as discussed earlier, the LPSO also serves to act as a short-fiber reinforcement (*3*).

In general, little difference was observed in the strength levels obtained in dynamic testing (figure 8) relative to those observed under quasi-static conditions. In contrast, a noticeable increase in total strain for samples tested under dynamic conditions was observed.

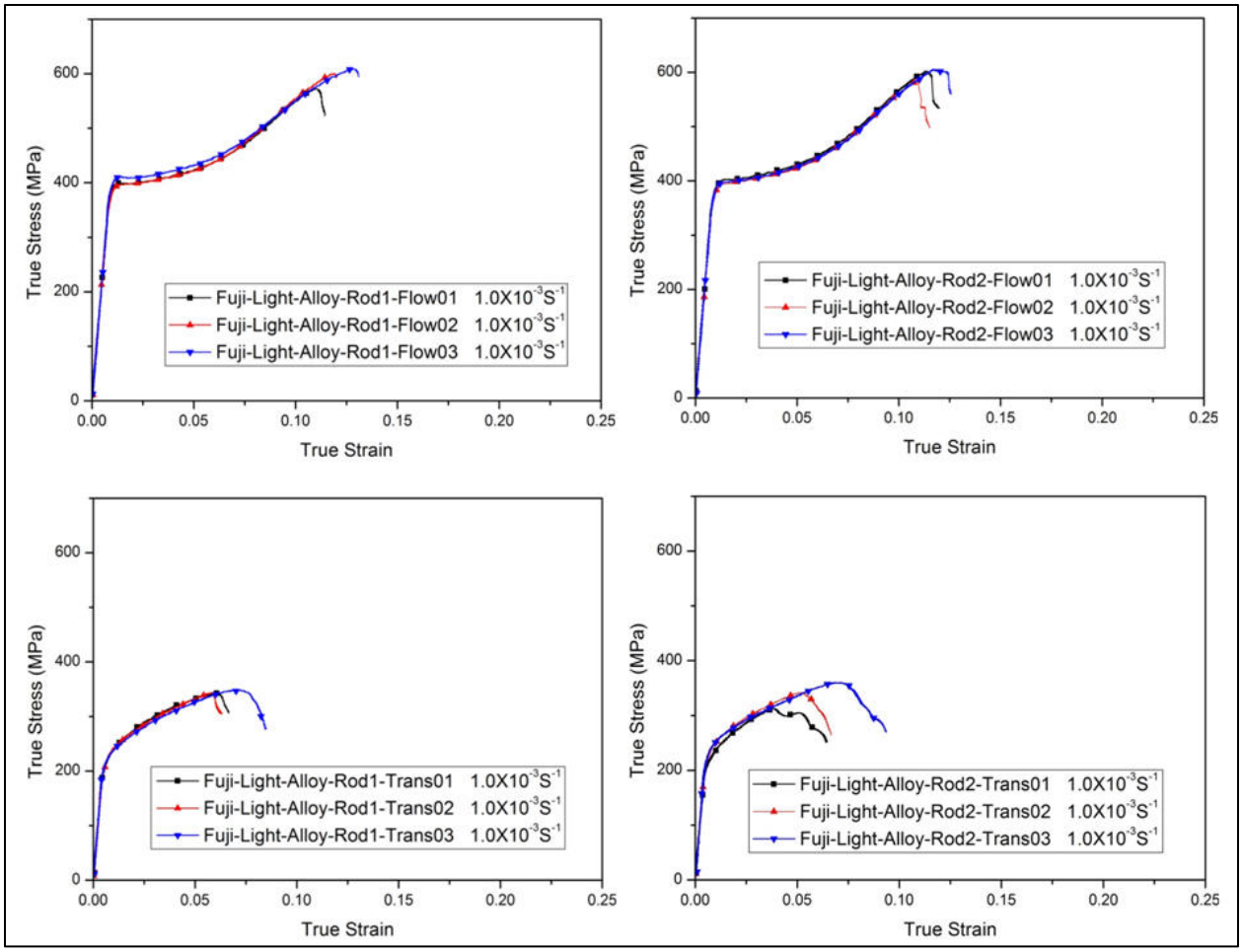

Figure 7. Quasi-static true stress–true strain curves along the flow and transverse directions. Flow direction shows an increasing strain hardening behavior after yielding. The strength is much lower in the transverse direction with limited strain hardening.

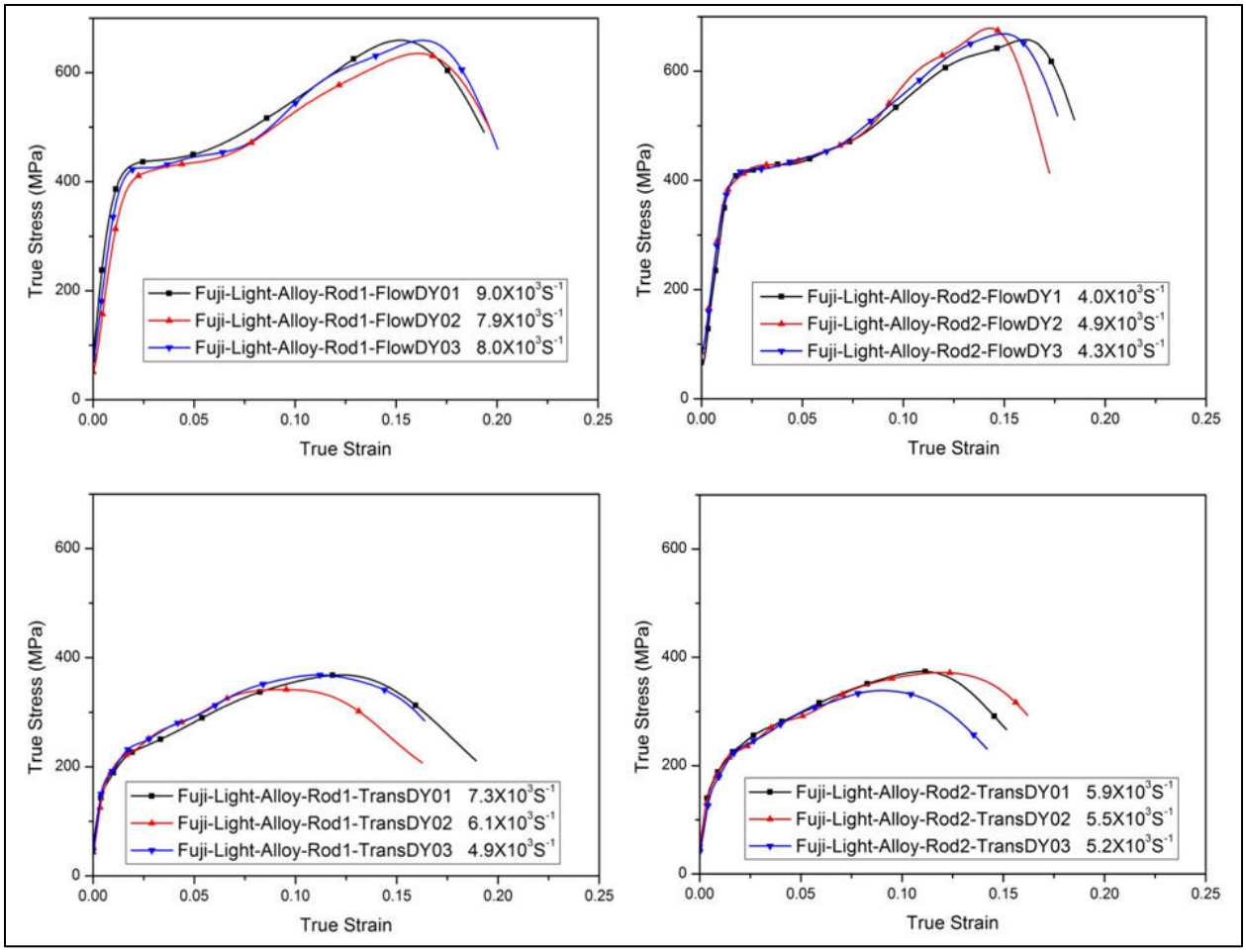

Figure 8. Dynamic true stress–true strain curves along the flow and transverse directions. The dynamic ultimate strength in both directions is slightly higher than that at quasi-static rate.

4. Accelerated Exposure and Electromechanical Testing

Corrosion testing was performed on round samples approximately 3 mm thick. After cutting, the samples were polished to 600 grit finish using conventional metallographic methods. The corrosion performance of the alloy was then determined using the neutral salt fog testing method in accordance with ASTM Standard B117–Standard Practice For Operating Salt Spray (Fog) Apparatus (*15*). Testing was performed at a temperature of 95 °F with saturated humidity and an atomized fog of 5% NaCl solution. The samples were observed after 1, 2, 4, 8, 24, 72, and 168 h. A mass loss rate of 61.2 ± 11.2 mils per year (mpy) was calculated from the B117 data. The photographs shown in figure 9 for the two rods indicate that noticeable changes in surface appearance occur as soon as 24 h after the beginning of the test. Continued exposure results in

progressive changes in surface appearance due to the onset of corrosion. A comparison of the corrosion performance of the Fuji Light alloy relative to other recently studied Mg alloys is discussed in the next section.

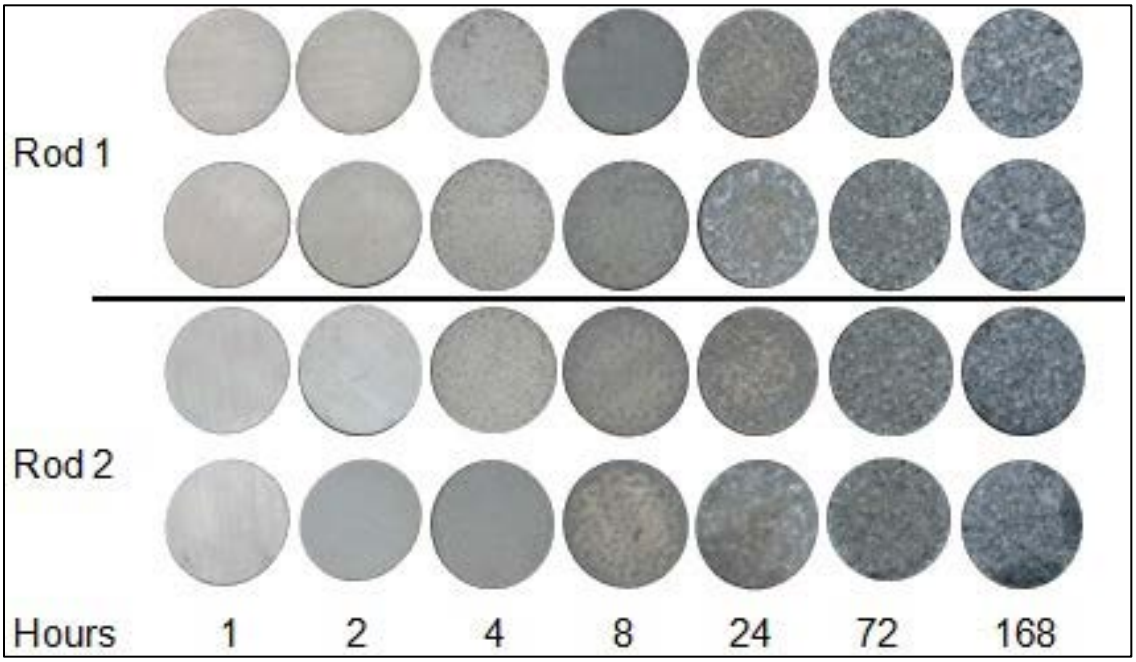

Figure 9. Optical photographs detailing changes in surface appearance after the indicated number of hours for the Fuji Light samples subjected to the salt fog test chamber.

Accelerated cyclic corrosion testing was performed according to standard GM9540P. In this method, the sample is exposed to an 18 stage cycle that is composed of the following: saltwater mist of 0.9% NaCl, 0.1% CaCl2, 0.25% $NaHCO_3$ solution; high humidity; ambient drying; and heated drying. The observation intervals for these samples were 1, 2, and 10 cycles. As part of the observation, the specimens were scanned at an 800-dpi optical resolution after any loose corrosion products present on the sample surface were removed via rinsing with deionized water. Examination of samples after 10 cycles revealed a general darkening of the sample, but no readily observable corrosion events.

Potentiodynamic polarization provides a reasonable method for qualitatively predicting the propensity of an alloy to suffer localized corrosion in the form of pitting and crevice corrosion. A typical experiment ramps the potential of the substrate relative to a reference electrode, such as the saturated calomel electrode (SCE), at a particular rate using a potentiostat. Typically, the starting voltage is 200–300 mV below the open circuit potential (OCP) and the ending voltage is typically above the OCP by >200 mV. The current observed in this polarization experiment corresponds to the rate at which the anodic or cathodic reactions are occurring. The potentiodynamic polarization measurement provides a qualitative representation of the alloy in a given solution and can be used to study regions of passivity, corrosion rate, and corrosion behavior in a variety of environments.

Figure 10 shows the potentiodynamic polarization curves obtained for the Fuji Light alloys tested in 10-mM NaCl solution. AZ31B, a relatively common Mg alloy, is also shown for comparison. Experimental results indicate little difference between the corrosion behavior of the two alloy systems. The corrosion current of the Fuji Light alloy samples is higher than that of AZ31B, which indicates they may be more prone to corrosion in NaCl solution.

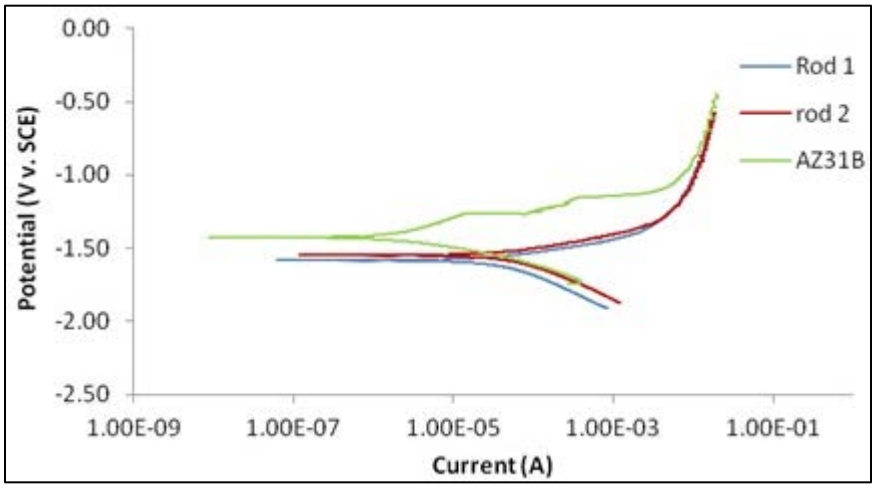

Figure 10. Potentiodynamic polarization curves obtained from two Fuji Light samples. This alloy appears to be more prone to corrosion than the AZ31B reference sample.

5. Comparison to Other Alloys

Over the last decade, ARL has conducted numerous efforts to characterize the mechanical and corrosion performance of commercially available Mg-based alloys. Furthermore, ARL has partnered with academia and industry to develop promising new alloys. Comparison of previous results with the present data would prove beneficial in determining the potential viability of this alloy for Army applications.

The performance of the Fuji Light alloy relative to other recently evaluated alloys is detailed in table 3. WE43 is a Y and RE containing alloy developed by Magnesium Elektron (Manchester, England) that has been evaluated in plate form for the indicated temper condition. AMX602 and ZAXE1711 are calcium containing alloys that are produced in powder form using the spinning water atomization process with the powders then extruded in rod form. Properties shown in the table are for samples extruded at a temperature of 250 °C.

Due to sample size limitations, comparisons of alloy performance are limited to the extrusion direction. Tensile testing of the Fuji Light alloy indicated that it had a yield strength of 350 MPa and an ultimate strength of 400 MPa with an elongation of approximately 8%. As seen in the

following table, the strength properties of the Fuji Light alloy are generally superior to the indicated alloys. However, the total elongation of the referenced alloys is superior to that measured for the current alloy.

Table 3. Mechanical properties of a selected number of new Mg alloys recently evaluated at ARL. Test results obtained in this study indicate that the Fuji-Light alloy typically has higher strengths but a lower elongation.

Alloy	TYS (MPa)	UTS (MPa)	Elongation (%)
WE43-F[a]	—	273	20.5
WE43-T5[a]	—	332	10.5
AMX602[b]	311	358	17.8
ZAXE1711[b]	269	380	18.2

[a]See reference 16. [b]See reference 17.

Regarding corrosion resistance, potentiodynamic polarization suggests that the corrosion resistance of the Fuji Light alloy is less than that of AZ31B. Shown in the following figure is the corrosion rate in mpy obtained using accelerated laboratory test methods for a wide range of Mg alloys (*18*, *19*). For the Fuji Light alloy, a mass loss of 61.2 ± 11.2 mpy was calculated from the B117 Neutral Salt Fog data (*15*). This value is the highest of any alloys shown in figure 11.

More importantly, the apparently poor corrosion resistance of this alloy is in direct contradiction to claims that assert the minor additions of Al and/or La would improve its corrosion resistance (*6*–*8*). However, a closer examination of these studies indicates that the Zn content is typically at 1% or less. Indeed, one report indicated the minimum corrosion rate occurred for a Zn content of approximately 0.75%—and that the corrosion rate began to increase considerably as the Zn content increased above 1% (*6*). Higher levels of Zn have also been reported to lead to an increased susceptibility to stress corrosion cracking (*20*). Thus, it appears that the higher zinc content of this alloy actually resulted in a reduced level of corrosion performance.

Before concluding that the Fuji Light alloy has poor corrosion performance, it is important to note that several factors may have influenced the present mass loss results. First, unlike the other alloys that were tested using square samples, the Fuji Light alloy had to be tested using cylindrical samples due to limited material availability. This is an important consideration, as the calculated mass loss rate can be affected by both geometry and testing procedures. Second, the corrosion products were not removed after each exposure measurement. As a result, the mass loss rate could be higher than currently measured due to the exposure of the fresh surface, which

could react at a faster rate than the covered surface. Thus, although it appears that the Fuji Light alloy experiences a higher corrosion rate than many other Mg alloys, further testing using a standardized specimen size/shape is needed before a definitive conclusion can be reached in this regard.

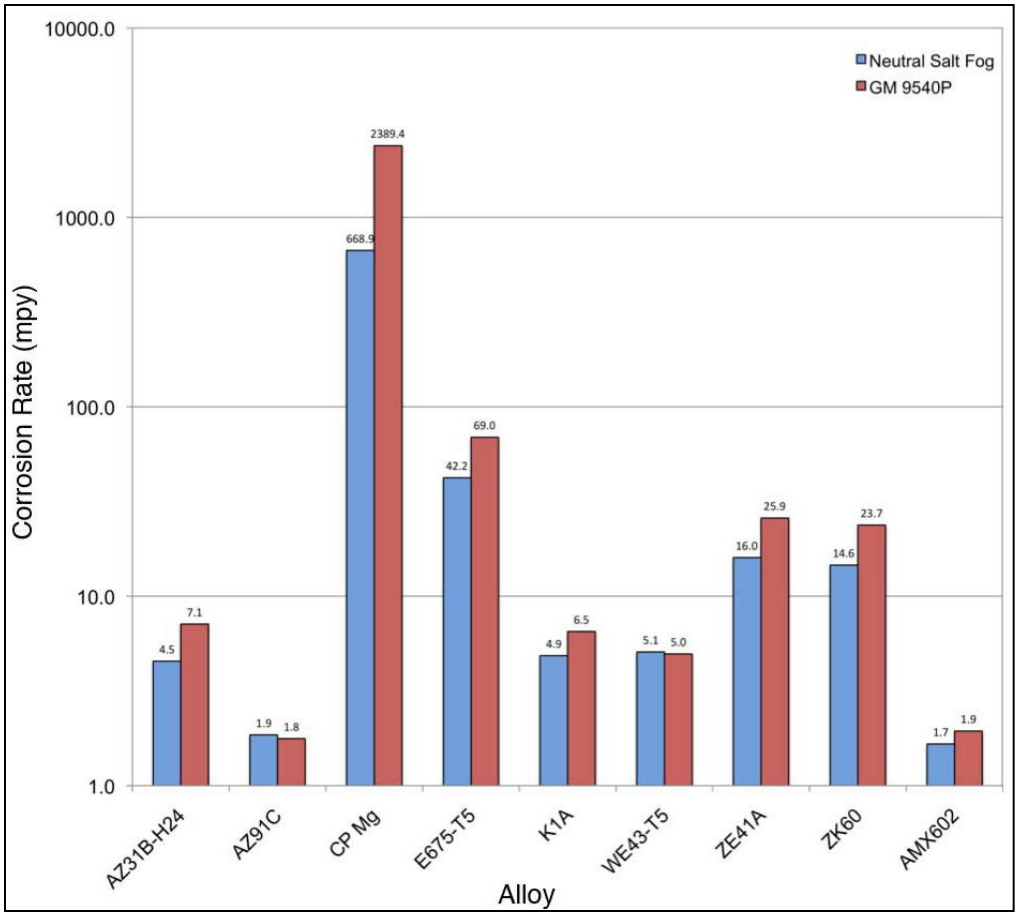

Figure 11. Corrosion rate in mpy for a range of Mg alloys. The observed value for Fuji Light alloy measured in Neutral Salt Fog (e.g., blue bar) is approximately 61, which makes it better than only Commercially Pure Mg in terms of corrosion rate.

6. Conclusions

This report has detailed the evaluation of the mechanical and electrochemical properties for an Al and La modified $MgZn_2Y_2$ alloy obtained from the Fuji Light Metal Company (Japan). This alloy is representative of the continued development of alloys based on the $MgZn_1Y_2$ alloy initially reported by Inoue (*1*). The tensile properties of the alloy were found to equal or exceed those of other Mg alloys that have been evaluated recently by ARL scientists. However, the initial results obtained from corrosion testing suggested that the alloy has poor corrosion

resistance. While the latter does not necessarily eliminate this alloy as one of further interest, it is a concern given the availability of Mg alloys with similar strengths and superior corrosion performance.

7. References

1. Inoue, A.; Kawamura, Y.; Matsushita, M.; Hayashi, K.; Koike, J. Novel Hexagonal Structure and Ultrahigh Strength of Magnesium Solid Solution in the Mg-Zn-Y System. *J. of Materials Research* **2001,** *16,* 1894.

2. Yoshimoto, S.; Yamasaki, M.; Kawamura, Y. Microstructure and Mechanical Properties of Extruded Mg-Zn-Y Alloys with 14H Long Period Ordered Structure. *Materials Transactions* **2006,** *47,* 959.

3. Hagihara, K.; Kinoshita, A.; Sugino, Y.; Yamasaki, M.; Kawamura, Y.; Yasuda, H. Y.; Umakoshi, Y. Effect of Long-Period Stacking Ordered Phase on Mechanical Properties of $Mg_{97}Zn_1Y_2$ Extruded Alloys. *Acta Materialia* **2010,** *58,* 6282.

4. Kawamura, Y.; Yamasaki, M. Formation and Mechanical Properties of $Mg_{97}Zn_1RE_2$ Alloys with Long-Period Stacking Ordered Structures. *Materials Transactions* **2007,** *48,* 2986.

5. Itoi, T.; Kuroda, Y.; Kawamura, Y.; Hirohashi, M. Preparation and Mechanical Property of MgZnY Alloy With A Long Period Ordered Phase. *Materials Science Forum* **2010,** *619,* 654–656.

6. Yamasaki, M.; Izumi, S.; Kawamura, Y. Development of High-Strength and Highly Corrosion-Resistant Bulk Nanocrystalline Mg-Zn-Y Alloys with Long Period Stacking Ordered Phase. *ECS Transactions* **2009,** *16,* 81.

7. Okouchi, H.; Seki, Y.; Sekigawa, T.; Hira, H.; Kawamura, Y. Nanocrystalline LPSO MgZnYAl Alloys with High Mechanical Strength and Corrosion Resistance. *Materials Science Forum* **2010,** *1476,* 638–642.

8. Izumi, S.; Yamasaki, M.; Kawamura, Y. Improvement of Corrosion Resistance of Extruded Mg-Zn-Y Mg/LPSO Two-Phase Alloys by Fourth Element Addition. *Materials Science Forum* **2010,** *767,* 654–656.

9. Catalano, J.; Kecskes, L. *A Generic Metallographic Preparation Method for magnesium Alloys;* ARL-TR-6447; U.S. Army Research Laboratory: Aberdeen Proving Ground, MD, 2013.

10. Kim, J.; Kawamura,Y. Influence of Rare Earth Elements on Microstructure and Mechanical Properties of $Mg_{97}Zn_1Y_1RE_1$ Alloys. *Materials Science & Engineering* **2013,** *A573,* 62.

11. Yamasaki, M.; Hasimoto, K.; Hagihara, K.; Kawamura, Y. Multimodal Microstructure Evolution in Wrought Mg-Zn-Y Alloys with High Strength and Increased Ductility. *Materials Science Forum* **2010,** *615,* 654–656.

12. Lou, X.; Li, M.; Boger, R.; Agnew, S.; Wagoner, R. Hardening Evolution of AZ31B Mg Sheet. *International J. of Plasticity* **2007,** *23*, 44.

13. Barnett, M. Twinning and the Ductility of Magnesium Alloys: Part I Tension Twins. *Materials Science & Engineering* **2007,** *A464*, 1.

14. Hagihara, K.; Kinoshita, A.; Sugino, Y.; Yamasaki, M.; Kawamura, Y.; Yasuda, Y.; Umakoshi, Y. Plastic Deformation Behavior of $Mg_{97}Zn_1Y_2$ Extruded Alloys. *Transactions of Nonferrous Metals Society of China* **2010,** *20*, 1259.

15. ASTM International B117-11. *Standard Practice for Operating Salt Spray (Fog) Apparatus*. October 2011.

16. Sano, T.; Yu, J.; Davis, B.; DeLorme, R.; Cho, K. In-Situ Scanning Electron Microscopy Comparison of Microstructure and Deformation between WE43-F and WE43-T5 Magnesium Alloys. In *Magnesium Technology; 2011; 2011 TMS Annual Conference*; Wim H. Sillekens, Sean R. Agnew, Neale R. Neelameggham, Eds. (TMS, 2011), Vol. Magnesium Technology 2011, pp. 345–348.

17. Jones, T.; Labukas, J.; Placzankis, B.; Kondoh, K. *Ballistic and Corrosion Analysis of New Military Grade Magnesium Alloys AMX602 and ZAXE1711 for Armor Applications;* ARL-TR-5931; U.S. Army Research Laboratory: Aberdeen Proving Ground, MD, 2012.

18. Placzankis, B.; Miller, C.; Mathaudhu, S.; DeLorme, R. Corrosion Comparisons among Magnesium Alloys of Interest for DoD Systems using Laboratory Based Accelerated Corrosion Methods (Paper #10085). Presented at the NACE Corrosion 2010 Conference and Expo, 2010.

19. Jones, T.; Placzankis, B. *The Ballistic and Corrosion Evaluation of Magnesium Elektron E675 vs. Baseline Magnesium Alloy AZ31B and Aluminum Alloy 5083 for Armor Applications;* ARL-TR-5565; U.S. Army Research Laboratory: Aberdeen Proving Ground, MD, 2011.

20. Zeng, R.; Zhang, Z.; Huang, W. -J.; Dietzel, W.; Kainer, K. U.; Blawert, C.; Wei, K. Review of Studies on Corrosion of Magnesium Alloys. *Transactions of Nonferrous Metals Society of China* **2006,** *16*, s763.

List of Symbols, Abbreviations, and Acronyms

ARL	U.S. Army Research Laboratory
EDS	energy dispersive spectroscopy
Gd	gadolinium
LPSO	long period stacking ordered
mpy	mils per year
OCP	open circuit potential
SCE	saturated calomel electrode
SEM	scanning electron microscope
Tb	terbium
Y	yttrium
Zn	zinc

NO. OF COPIES	ORGANIZATION
1 (PDF)	DEFENSE TECHNICAL INFORMATION CTR DTIC OCA
1 (PDF)	DIRECTOR US ARMY RESEARCH LAB IMAL HRA
1 (PDF)	DIRECTOR US ARMY RESEARCH LAB RDRL CIO LL
1 (PDF)	GOVT PRINTG OFC A MALHOTRA

ABERDEEN PROVING GROUND

4 (PDF)	DIR USARL RDRL WMM F V H HAMMOND B G BUTLER RDRL WMM B T SANO RDRL WMM C J P LABUKAS